Water Science & Technology

IWA PUBLISHING

Water Science & Technology Vol 93 No 12, 1802 doi: 10.2166/wst.2026.299

Pyrolysis temperature shapes the structure and filtration capacity of spent-coffee-ground biochar for 1-μm microplastics and bacteria removal from wastewater

Alessia Torboli [a,*], Luca Fiori [a,b], Riccardo Ceccato [c], Devid Maniglio [d], Laura Bruni [e] and Paola Foladori [a,b]

[a] Center Agriculture Food and Environment (C3A), University of Trento, via Edmund Mach 1, San Michele all'Adige, Trento 38098, Italy
[b] Department of Civil, Environmental and Mechanical Engineering, University of Trento, via Mesiano 77, Trento 38123, Italy
[c] Department of Industrial Engineering, University of Trento, Via Sommarive 9, Trento 38123, Italy
[d] Center for Biomedical Technologies (BIOtech), Department of Industrial Engineering, University of Trento, Via delle Regole 101, Mattarello, Trento 38123, Italy
[e] ADEP, Agenzia per la Depurazione (Wastewater Treatment Agency), Autonomous Province of Trento, via Gilli 3, Trento 38121, Italy
*Corresponding author. E-mail: alessia.torboli@unitn.it

AT, 0009-0009-1284-3172; LF, 0000-0003-0585-3793; RC, 0000-0001-7281-0449; DM, 0000-0002-1653-861X; LB, 0009-0000-4711-2315; PF, 0000-0002-7483-0416

ABSTRACT

Small microplastics are an increasing environmental concern due to their high mobility, large surface area-to-volume ratio, and ability to transport co-contaminants and microorganisms. Yet, particles in the 1-μm range remain difficult to quantify and remove, and standardized approaches to evaluate treatment performance are still lacking. This study addresses this methodological gap by combining controlled microplastic spiking in real secondary-treated wastewater with high-throughput flow cytometry for rapid quantification of 1-μm fluorescent microplastics and SYBR Green I-stained bacteria. Spent coffee grounds biochar produced at 300, 500, and 700 °C was evaluated in rapid small-scale column tests (1 mL min^{-1}; sampling every 2 min) to investigate how pyrolysis temperature influences structure and removal efficiency. Biochar produced at 500 °C achieved nearly complete removal of 1-μm microplastics and retained approximately 90% of bacteria, outperforming materials produced at 300 and 700 °C, which showed reduced performance consistent with lower surface area and pore development. Breakthrough data from a long-term test were fitted using a lag-corrected Yoon–Nelson model, accurately predicting 50% breakthrough at 500 min and an estimated sorption capacity of 200 mg g^{-1}. These results demonstrate that tuning biochar production and integrating rapid analytical tools enable systematic optimization of sustainable filtration strategies for emerging micropollutants.

Key words: biochar-based filtration, flow cytometry, microplastics removal, rapid small-scale columns, wastewater treatment

HIGHLIGHTS

- Biochar from spent coffee grounds was produced at 300–700 °C for sustainable filtration.
- Flow cytometry enabled rapid quantification of 1-μm microplastics (MPs) and bacteria in wastewater.
- Microporosity, pore volume, and surface area are maximized at mild pyrolysis temperatures.
- Biochar produced at 500 °C achieved optimal material properties and >99% MP removal.
- A lag-corrected Yoon–Nelson model accurately predicted column breakthrough.

GRAPHICAL ABSTRACT

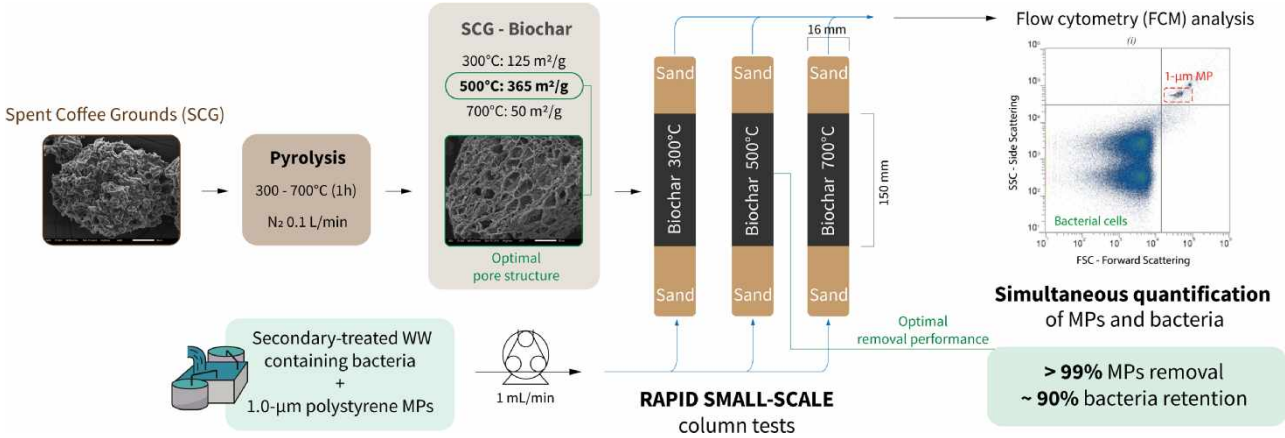

1. INTRODUCTION

Every day, wastewater (WW) treatment facilities discharge treated effluent containing traces of micropollutants unintentionally introduced into the sewer system, which are not completely removed during the treatment process and thus reach the environment. Among these, microplastics (MPs) (1 μm–5 mm) have emerged as widespread pollutants found in both our water systems and everyday life, with recent studies documenting their ubiquity across freshwater, marine, and even atmospheric compartments (Windsor *et al.* 2019). Numerous investigations have identified wastewater treatment plants (WWTPs) as one of the primary sources for MPs entering natural water bodies, ultimately reaching aquatic bodies if not properly removed (Liu *et al.* 2021; Monira *et al.* 2023). Current WWTPs are not specifically designed to remove MPs present in raw WW. Nevertheless, recent reviews report mean removal efficiencies of approximately 88% in secondary treatment, increasing up to 99.9% in tertiary processes for MPs detectable with conventional analytical methods (Reza *et al.* 2023). However, this apparent effectiveness is strongly dependent on the particle size. Most existing studies document particles in the tens to hundreds of micrometres range (Ziajahromi *et al.* 2017; Dronjak *et al.* 2023), leaving a significant knowledge gap at the <20 μm. In particular, the fate and removal of much smaller MPs around 1 μm remain poorly understood, where conventional detection and capture approaches become increasingly challenging. Although overall removal rates appear robust, studies examining different size ranges often report markedly different efficiencies (Ormaniec 2024). Moreover, during WW treatment, degradation and fragmentation can reduce MP size (Hajji *et al.* 2023), leading to a higher proportion of smaller particles in the treated effluent compared with those retained in sludge or within the treatment system (Iordachescu *et al.* 2024), and this ultimately affects retention efficiency. Recent investigations further highlight that even high removal efficiencies in WWTPs may still result in significant environmental loads due to the massive volumes of treated effluent discharged daily, particularly for smaller MPs that escape conventional retention mechanisms (Wang *et al.* 2024).

Sub-micron MPs pose a critical challenge because their small size enhances hydrodynamic mobility, reduces sedimentation rates, and facilitates long-range transport across aquatic compartments (Guo *et al.* 2024). Their high surface area-to-volume ratio promotes interactions with dissolved organic matter and microbial communities, increasing the likelihood of biofilm formation and the co-transport of attached contaminants or microorganisms (Ali *et al.* 2024). In fact, their surfaces offer ideal sites for bacterial attachment, leading to the formation of biofilms that transform MPs into microbial 'hotspots'. This phenomenon, referred to as 'microplastisphere', has been widely reported in aquatic environments (Zettler *et al.* 2013; Costigan *et al.* 2022). Such colonization has major ecological and health implications. MP-associated biofilms can host potentially pathogenic or antibiotic-resistant bacteria (Jia *et al.* 2024), which benefit from the extracellular polymeric substance (EPS) matrix that acts as a protective barrier against environmental stresses and antimicrobial agents (Flemming *et al.* 2023). As plastics age and weather, they show increased surface roughness, functional groups, and hydrophobicity, all of which promote further attachment of bacteria, as well as the further adsorption of organic contaminants and metals (Bhagwat *et al.* 2021). Rummel *et al.* (2017) showed that biofilm growth on MPs can also significantly alter their density, thereby affecting their settling velocity and resuspension, and consequently, the transport mechanism. As a result,

biofilm-coated MPs become heavier, more aggregated, and more stable, and this can affect their removal in engineered systems and contribute to their persistence in the environment.

Given their uncertain abundance, high mobility, and potential for carrying other contaminants, small MPs urgently require new treatment solutions. Conventional methods such as membrane filtration, coagulation, or activated carbon are often energy or chemical intensive and still struggle with the smallest size fractions (Zhang *et al.* 2021). Biochar, a carbon-rich material produced from renewable biomass through pyrolysis (i.e. a thermal treatment occurring at hundreds of Celsius degrees under inert – typically N_2 – atmosphere), has recently gained attention as a sustainable alternative (Ji *et al.* 2024). Biochar is low-cost, highly porous, and chemically tuneable, and can be obtained from diverse organic wastes, including spent coffee grounds (SCGs), as in the present research. Importantly, its performance is highly dependent on its production conditions, particularly the feedstock type and pyrolysis temperature (Ippolito *et al.* 2020). Higher pyrolysis temperatures typically enhance pore development and surface area, often modifying surface chemistry and wettability, thereby improving affinity for small hydrophobic particles, including nanoplastics and MPs (Cairns *et al.* 2024; Li *et al.* 2024), as well as microbial retention (Fady *et al.* 2025). Several studies have demonstrated the potential of biochar for MP removal from water (*inter alia* Hsieh *et al.* (2022)). For example, rice-husk-derived biochar integrated into sand filters significantly reduced (~98%) spiked 1-μm MPs under laboratory column conditions (Parashar & Hait 2024), while agricultural waste–derived biochar achieved 86–93% removal of MPs (>45 μm) from synthetic runoff water (Olubusoye *et al.* 2024). In another recent study using spiked MPs between 1 and 5 μm, biochar outperformed rapid sand filters by retaining nearly all particles in the 2–5 μm range, whereas 1-μm MPs remained more difficult to remove (~50% efficiency), highlighting the challenge of filtering the smallest fractions (Torboli *et al.* 2025).

Despite these advances, few studies have focused on optimized biochar properties specifically for the removal of MPs at the 1-μm scale. One major limitation lies in the difficulty of detecting and quantifying the smallest MPs naturally present in WW, where concentrations fluctuate and are often too low for reproducible experiments. To overcome this constraint, artificial microspheres can be spiked into real WW matrices as traceable surrogates to investigate MP transport and removal mechanisms under controlled yet environmentally relevant conditions (Foladori *et al.* 2025). For representative experiments, these model particles should be made of common polymers (i.e. polystyrene) and reflect shapes observed in WW effluents, such as microbeads (Hidayaturrahman & Lee 2019; Adhikari *et al.* 2022). The use of fluorescent tracers has increasingly been applied to investigate MP transport and fate in aquatic systems, enabling controlled tracking of particle behaviour in complex matrices (Cook *et al.* 2020). While these approaches have advanced our understanding of MP transport in natural systems, their integration into engineered treatment studies remains limited. Moreover, although growing evidence highlights the ecological relevance of MP and microbe interactions in aquatic environments (Dykes *et al.* 2026), few engineering studies have addressed their simultaneous quantification and removal within WW treatment systems.

Against this background, the present study addresses two main challenges: (i) the detection and quantification of small MPs in WW through the spiking of traceable 1-μm microspheres, coupled with the simultaneous enumeration of naturally occurring bacterial cells stained with a specific fluorochrome for flow cytometry (FCM) analysis; and (ii) the development of an optimized, scalable, and sustainable filtration system capable of effectively removing ultrafine MPs before their discharge into natural waters. To examine the effect of pyrolysis temperature on biochar properties, three representative regimes were selected: 300 °C as the lower limit of biochar formation, 500 °C to assess whether moderate conditions are sufficient to optimize structural development and filtration performance, and 700 °C to determine whether further carbonization yields proportional benefits or simply increases energy demand (Wang & Wang 2019). The high-throughput capability of FCM, enabling the analysis of thousands of particles per sample within minutes, provides the analytical resolution necessary to systematically evaluate how biochar production conditions influence removal performance at the most challenging size scale. In doing so, this study supports the development of low-cost and sustainable filtration technologies targeting emerging micropollutants in WW.

2. METHODS

2.1. Biochar production and characterization

Dried SCGs were pyrolyzed in a nitrogen-purged (0.1 L min^{-1}) horizontal furnace at three target temperatures: 300, 500, and 700 °C. The heating rate was set to 7 °C min^{-1}, with a residence time of 1 h at the target temperature. Each pyrolysis condition was conducted in duplicate to ensure statistical robustness of yield and subsequent analyses. Biochar yield was

determined by comparing the dry weight of SCG before and after pyrolysis. After cooling, the obtained biochar was washed with deionized (DI) water (solid-to-liquid ratio = 1:10 w:v) to remove soluble impurities from its surface. The pH of the washing solution was simultaneously monitored to assess the surface acidity or alkalinity of the biochar.

Physicochemical and morphological properties were then analyzed to evaluate the influence of pyrolysis temperature. Elemental composition (C, H, N) was determined using a LECO CHN628 carbon/hydrogen/nitrogen determinator. Ash content was determined using an ISO 18122-based method adapted for biochar according to European Biochar Certificate recommendations. Oxygen content was consequently calculated by difference (O = 100 – C – H – N – ash). Functional groups were identified by Fourier-transform infrared (FTIR) spectroscopy in the 4,000–400 cm^{-1} range (Agilent Cary 630 FTIR Spectrometer).

Wettability was evaluated by measurement of the contact angle in DI water using sessile drops (3 μl, five samples) and analyzing using the ImageJ plugin (Stalder *et al.* 2006). To perform the measure, the materials were compacted into pellets using a stainless-steel mold and a press (13 tonnes), in order to minimize the effects of powder surface roughness and the contribution of air trapped between the powder grains, which in hydrophobic materials generally determines an overestimation of the contact angle.

Microstructural characteristics of the biochars were assessed through granulometric analysis (Malvern Panalytical Mastersizer 3000+). Specific surface area values, according to the Brunauer–Emmett–Teller method, and pore size distribution curves, according to the density functional theory (DFD)-derived method, were calculated for the three types of biochar. Pyrolyzed samples at 300 and 500 °C were analyzed by means a 3Flex (Micromeritics, Alfatest) instrument. Analyses were performed in gaseous carbon dioxide atmosphere operating at 273 K, according to the IUPAC Technical Guidelines for microporous materials (IUPAC Technical Report, Thommes *et al.* 2015) up to 0.035 P/P_0 relative pressure. On the other hand, sample treated at 700 °C was analyzed by means an Autosorb 6300 (Anton Paar) instrument, operating with nitrogen at 77.35 K. Morphology was finally observed by scanning electron microscopy (SEM; JEOL JSM-IT300LV).

At the end of the filtration tests in the rapid small-scale columns, biochar was collected from the columns, dried, and re-characterized following the analytical procedures described earlier.

2.2. Water matrix investigated

The water matrix used in this study is secondary-treated WW collected at the outlet of the full-scale municipal WWTP of Trento Nord (Italy) before the effluents are discharged into the receiving river. The plant serves a population equivalent of 120,000 and processes an average flow rate of 21,000 m^3/d and an average organic load of 11,000 kg COD/d (chemical oxygen demand). The layout of the plant (Supplementary material, Figure S1) comprises mechanical pre-treatments (fine screening, grit chamber) followed by primary settling (2,478 m^3). Then, the biological treatment consists of an activated sludge stage (4,200 m^3) followed by secondary settlers (5,648 m^3). The physicochemical characterization of collected WW is detailed in Table 1.

Table 1 | Physicochemical characterization (avg. ± st. dev.) of secondary-treated wastewater collected in the Trento Nord WWTP

Parameter	Units	WW concentration (avg. ± st. dev.)
COD	mg/L	25 ± 0.0
BOD_5	mg/L	6.6 ± 2.2
TSS	mg/L	0.5 ± 0.0
TKN	mg/L	4.8 + 0.6
NH_4^+-N	mg/L	2.6 ± 1.2
NO_3^--N	mg/L	13.5 ± 3.5
NO_2^--N	mg/L	0.9 ± 0.1
Total N	mg/L	18.5 ± 4.9
Total P	mg/L	1.4 ± 0.3
Temperature	°C	17.6 ± 4.5
pH	–	7.7 ± 0.1

Note: BOD_5, biochemical oxygen demand; TKN, total Kjeldahl nitrogen; TSS, total suspended solids.

2.3. Fluorescent MPs and bacteria staining

Polystyrene 1-μm spherical particles Fluoro Max™ G0100 (Thermo Fisher, USA; excitation λ_{ex} = 468 nm, emission λ_{em} = 508 nm) were used as traceable MPs as they contain internally embedded green fluorophores, ensuring stable fluorescence emission that can be easily detected by FCM without dye leaching during experiments. MPs were added into secondary-treated WW to achieve an initial concentration of 0.80 ± 0.05 mg/L, corresponding to 1,430 ± 90 MP/μL. These concentrations in the working suspension were measured in triplicate using FCM.

For the enumeration of bacterial cells naturally present in the WW, WW samples before and after filtration were stained with the fluorochrome SYBR Green I (Thermo Fisher Scientific, USA). SYBR Green I is one of the most sensitive stains for detecting double-stranded DNA in cells, able to produce bright green fluorescence when cells are excited under a blue laser (λ_{ex} = 495 nm, λ_{em} = 525 nm). The working solution was prepared by diluting the dye commercial stock 1:30 in dimethyl sulfoxide. An aliquot of 10 μL of the working solution was added to 1 mL of the WW samples to stain bacterial cells. Then, the samples were incubated for 15 min at room temperature in the dark before FCM analysis. It is worth noting that SYBR Green I is a nucleic acid stain that penetrates all cell membranes, regardless of their integrity or damage, thus providing a count of total cells, including both live and dead cells.

2.4. Flow cytometry and enumeration of 1.0-μm MPs and bacteria

For FCM analyses, *Attune NxT* Acoustic Focusing Flow Cytometer (Thermo Fisher, USA) equipped with a 488 nm laser was used. WW samples were filtered using 20-μm filters (CellTrics, Partec) to remove coarse solids that could clog the flow cytometer nozzle. Signals of scattering and green fluorescence were collected for each particle passing through the flow chamber and in front of the laser of the cytometer.

The FCM analysis procedure was based on the following steps: (i) blank analysis to establish signal thresholds and eliminate background noise; (ii) setting the WW flowrate to 25 μL min^{-1}; (iii) acquisition of a minimum of 50,000 events for each WW sample to ensure statistically representative data; (iv) collection of forward scattering (FSC), side scattering (SSC), and green fluorescence (FL1) signals. Finally, histograms/cytograms were plotted to differentiate MPs from stained bacterial cells.

2.5. Rapid small-scale column tests with SCG-biochar

Three identical glass columns (16 mm internal diameter) were packed with a 150 mm layer of SCG-biochar, positioned between two 100 mm layers of sand (2–4 mm) to prevent biochar loss. Sequential pore volumes (PVs; 10 mL each), defined as the volume of solution required to completely fill the column empty space, were injected from the bottom using a peristaltic pump to ensure controlled flow conditions.

The filtration tests consisted of five main phases:

(i) Pre-equilibration: 10 PVs of distilled water were injected at 10 mL min^{-1} to achieve complete wetting of the material and remove trapped air.
(ii) Conditioning: three PVs of WW were introduced.
(iii) Spiking: four PVs of WW spiked with 1-μm MPs (0.8 mg L^{-1}) were injected.
(iv) Elution: a further six PVs of WW were added to allow suspended MPs to elute.
(v) Washing: three PVs of distilled water (10 mL min^{-1}), alternated with air (5 L min^{-1}), were applied three times for backwashing of the filters and evaluate the consequent leaching of MPs and bacterial cells.

Phases (ii), (iii), and (iv) were conducted at a flowrate of 1 mL min^{-1}, providing a contact time of approximately 10 min. Effluent samples were collected every 2 min for FCM analysis and construction of breakthrough curves. The release rate was calculated as the ratio between outlet and inlet concentrations (C_t/C_0). These rapid column tests were aimed at identifying the biochar production temperature that yielded the highest removal efficiency.

Then, the best type of biochar was used for performing a long-time filtration test (up to 50 PVs) by applying WW spiked with 1-μm MPs at 1.6 mg L^{-1} (double the previous concentration) and a constant flowrate of 1 mL min^{-1}. Samples were collected and analyzed every 10 min.

A stepwise schematic of the methodological workflow is presented in Figure 1, illustrating the sequence from biochar production to dynamic column testing, particle quantification, and modelling: To describe the breakthrough behaviour,

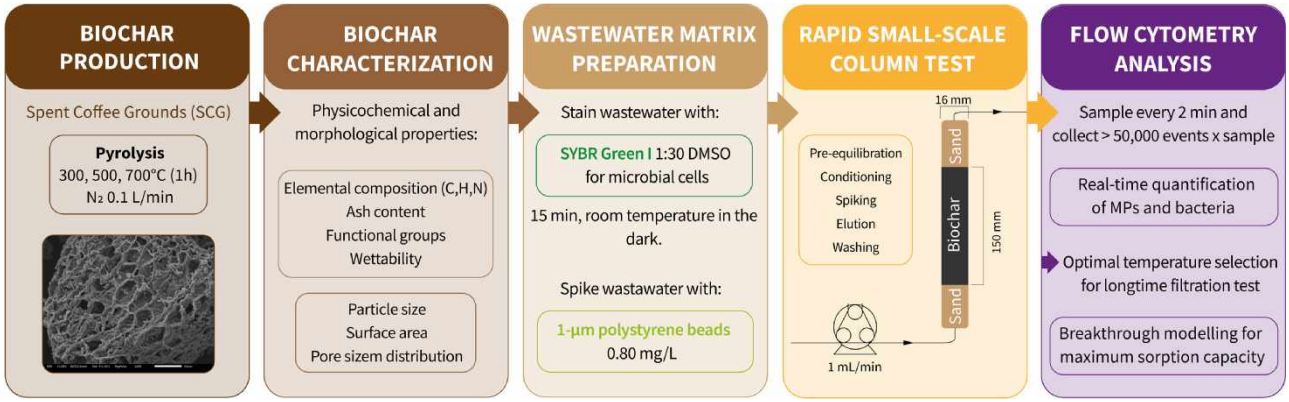

Figure 1 | Stepwise schematic representation of the experimental workflow, including biochar production at different pyrolysis temperatures and characterization, rapid small-scale column filtration of secondary-treated wastewater (WW) spiked with 1-µm MPs, real-time quantification of MPs and bacteria by FCM, and breakthrough curve modelling for performance evaluation.

filtration data were fitted using the Yoon–Nelson and Thomas kinetic models (Yoon & Nelson 1984; Thomas 1944), which are commonly applied to predict adsorption kinetics and column performance in fixed-bed systems.

The Yoon–Nelson model is based on the following mathematical expression:

$$\frac{C_t}{C_0} = \frac{1}{1 + e^{(k_{YN} \times (\tau - t))}}$$

while the Thomas model is expressed as follows:

$$\frac{C_t}{C_0} = \frac{1}{1 + e^{\left(\left(\frac{k_{TH} \times q_0 \times W}{Q}\right) - (k_{TH} \times C_0 \times t\right)}}$$

The Yoon–Nelson model assumes that the probability of adsorbate breakthrough decreases exponentially with time and does not require detailed information about the adsorbent characteristics or the adsorption mechanism. Its main parameters are the rate constant k_{YN} (h^{-1}) and the time required for 50% adsorbate breakthrough (τ, min). This simplicity makes it suitable for predicting column performance under different operating conditions.

Conversely, the Thomas model is derived from the Langmuir adsorption–desorption principle and assumes plug flow and negligible axial dispersion. It provides two key parameters: the rate constant k_{TH} (mL min^{-1} mg^{-1}) and the maximum adsorption capacity of the adsorbent q_0 (mg g^{-1}). The model correlates experimental data, including the weight W of the total adsorbent (g) and the flow rate Q in the column (mL min^{-1}), with theoretical adsorption behaviour, enabling estimation of the column's saturation capacity and efficiency. Both models can describe breakthrough curves over a wide range of conditions, offering insights into the kinetics and potential rate-limiting mechanisms of MP retention in biochar-packed columns.

2.6. Statistical analysis

An independent samples *T*-test was used to assess statistical differences between the mean effluent concentrations from the rapid small-scale column tests. The Shapiro-Wilk test was employed to confirm the normality of the dataset. In cases where the data did not meet the normality assumption, the nonparametric Mann–Whitney *U* test was applied as an alternative to assess statistical differences. The statistical significance was assessed at a probability level of $p < 0.05$ for the test.

One-way analysis of variance (ANOVA) was employed to analyze the statistical significance of the effect of pyrolysis temperature on filtration performance. Levene's test was employed to assess the homogeneity of variances. Following ANOVA, Tukey's honestly significant difference test was performed as a *post hoc* analysis to identify homogeneous groups among the experimental conditions. Statistical significance was determined at a probability level of $p < 0.05$ for all tests.

All the statistical tests were computed using Jamovi (version 2.3.28.0; The Jamovi Project), an open-source statistical software built on R.

3. RESULTS AND DISCUSSION

3.1. Characterization of SCG-biochar produced at different temperatures

Pyrolysis temperature exerts a major influence on biochar yield, surface chemistry, and structural properties. SCG were pyrolyzed at 300, 500, and 700 °C, and the main physicochemical characteristics of the resulting biochars are summarized in Table 2.

SCG demonstrated high potential as a feedstock for biochar production, with higher pyrolysis temperatures reducing yield due to the release of volatile matter and non-condensable gases. In detail, the mass yield on a dry basis passes from 57.1% at 300 °C to approximately 27% at 500 and 700 °C. In contrast, the biochar pH became progressively more alkaline, increasing from 4.9 at 300 °C to 8.5 at 700 °C, reflecting the concentration of ash and basic surface oxides at higher temperatures. The mean particle diameter (D_{50}) of all the pyrolysed biochars was 377 ± 15 μm (Table 2), with higher pyrolysis temperatures promoting a partial fragmentation of some granules, as shown by the granulometric distributions in Figure S2.

Elemental analysis (C, H, N), employed to assess the purity and chemical composition of biochar, revealed carbon as the dominant element (>67%), with variations depending on the biochar production temperature (Table 2) as volatile fractions are driven off. Hydrogen and nitrogen decreased progressively with increasing pyrolysis temperature, reflecting progressive dehydration and devolatilization during carbonization. The marked drop in hydrogen – from 7.2% at 300 °C to below 4% above 500 °C – can be attributed to the gradual fragmentation of the hydrogen-bond network in lignocellulosic polymers and loss of hydroxyl groups (Harvey *et al.* 2012). The ash content increased with pyrolysis temperature, reflecting the progressive concentration of inorganic constituents following organic matter degradation.

The analysis of functional groups (Figure 2(a)) revealed that unheated SCG and 300 °C biochar share similar functional features, with distinct peaks at 3,000–2,800 cm^{-1} associated with the stretching modes of aliphatic C-H_n groups. These peaks disappear in biochar originated at higher temperatures, indicating thermal decomposition of cellulose, hemicellulose, and lignin. As these biopolymers degrade, the rapid release of volatiles creates active sites that contribute to micro- and mesopores development, while surface oxygenated groups are progressively lost, as revealed also by the disappearance of the sharp peaks in the range of 1,800–1,700 cm^{-1} (C = O bonds) and in the range of 1,200–1,000 cm^{-1} (C-O bonds). In particular, the biochar produced at 700 °C becomes a material with a highly carbonized, nearly graphitic character due to the almost complete removal of surface functional groups, as typically observed for high-temperature carbonaceous materials (Tomczyk *et al.* 2020). This structural evolution is further supported by the very low atomic *H/C* ratio (Table 2), which is consistent with the progressive aromatization and condensation of the carbon matrix at elevated pyrolysis temperatures (Dong *et al.* 2025).

SEM observations support these findings: the surface of the 300 °C biochar remains coarse and relatively homogeneous (Figure 2(d)), more similar to unheated SCG (Figure 2(c)). In contrast, higher pyrolysis temperatures enhance porosity, producing the sponge-like morphology observed in the 500 and 700 °C biochars (Figure 2(e) and 2(f)).

These observations are consistent with the increase in surface area from 125 $m^2\ g^{-1}$ at 300 °C to 365 $m^2\ g^{-1}$ at 500 °C (Table 2), reflecting extensive micropore development (Figure 2(b)), followed by a marked decline to 50 $m^2\ g^{-1}$ at 700 °C. As microporosity was assessed through CO_2 physisorption for the 300 and 500 °C samples, the resulting surface area represents an apparent value that captures contributions from ultramicropores. In the case of untreated SCG, no significant

Table 2 | Comprehensive characterization of SCG-biochars produced at 300, 500, and 700 °C

Pyrolysis temp. (°C)	Yield (%)	pH (–)	Elemental composition							Granulometry			Pore distribution	
			C (%)	H (%)	N (%)	O (%)	Ash (%)	H/C	O/C	D_{10} (μm)	D_{50} (μm)	D_{90} (μm)	A_p (m^2/g)	V_p (cm^3/g)
300	57.1 ± 2.2	4.9 ± 0.7	67.6	7.2	3.2	18.9	3.0	1.3	0.21	152	393	1,077	125	0.039
500	27.7 ± 1.7	7.6 ± 0.2	74.1	3.9	3.8	12.3	4.6	0.6	0.12	217	365	610	365	0.097
700	26.9 ± 0.2	8.5 ± 0.3	73.7	2.7	2.5	15.1	6.1	0.4	0.16	194	373	702	50	0.015

Note: The table reports yield, pH, elemental composition (C, H, N, O, ash, reported as percentage by mass; H/C and O/C atomic ratios), particle-size distribution (D_{10}, D_{50}, D_{90}), pore structural characteristics (total pore area, A_p; total pore volume, V_p).

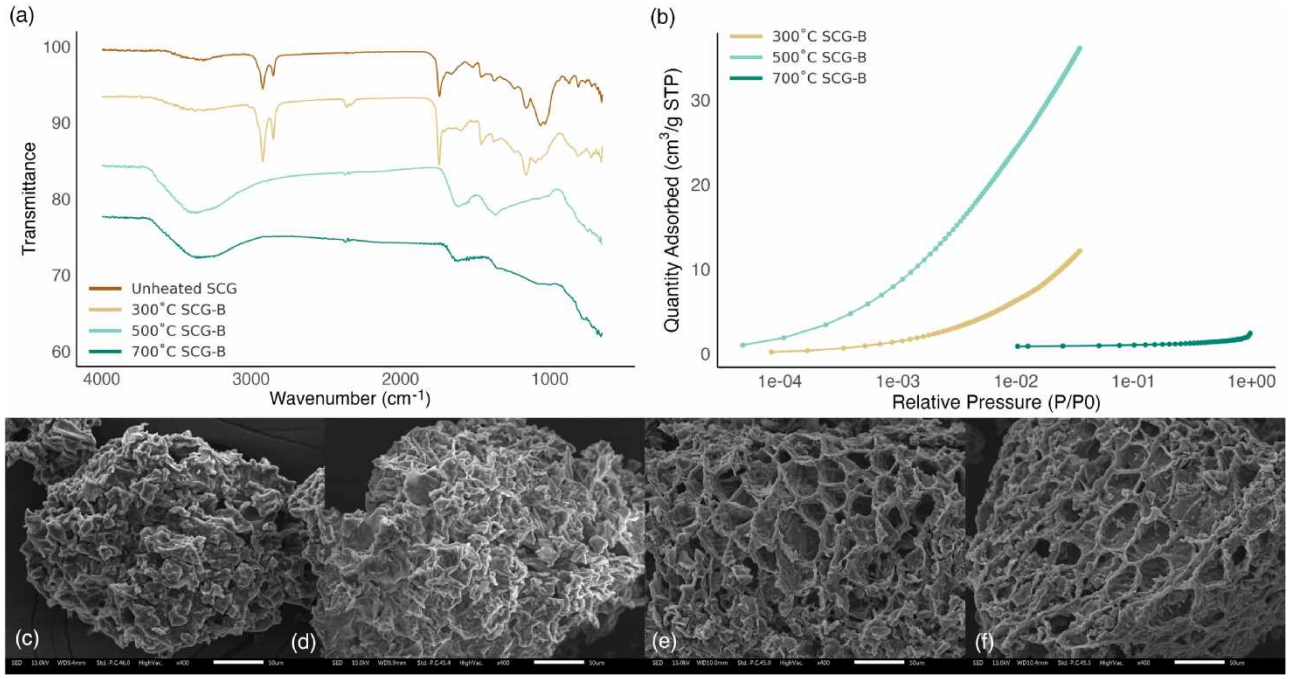

Figure 2 | (a) FTIR spectra, (b) physisorption isotherms, and SEM images at magnification 400× of (c) unheated SCG and SCG-biochar produced at (d) 300°C, (e) 500°C, and (f) 700 °C.

CO_2 adsorption was detected, indicating the absence of a developed ultramicroporous structure under the applied analytical conditions. The analysis confirmed that both the 300 and 500 °C biochars are predominantly microporous (Figure 2(b)), exhibiting type I physisorption isotherms according to the IUPAC nomenclature for adsorption isotherms and hysteresis loops (Thommes *et al.* 2015). Type I isotherms, typical of microporous materials, are defined by a steep adsorption uptake at low relative pressures, reflecting rapid pore filling and strong adsorbate–adsorbent interactions, followed by a plateau corresponding to micropore saturation (Figure 2(b)). Such behaviour is commonly reported for lignocellulosic biochars produced at intermediate pyrolysis temperatures, where the development of microporosity formed during thermal decomposition dominates the adsorption profile (Kuloglija *et al.* 2026). In particular, at 500 °C, pores smaller than 0.4 nm decrease, consistent with thermal restructuring of the carbon matrix, and the pore size distribution becomes markedly polymodal, with a pronounced increase in porosity at approximately 0.4 and 0.6 nm (Figure S2).

In contrast, the 700 °C biochar shows an intermediate isotherm between type I and type II, indicating a progressive loss of microporosity toward the development of non-porous or macroporous domains, where adsorption proceeds via multilayer formation on external surfaces rather than pore filling (Thommes *et al.* 2015). Consistently, both the total adsorbed volume (Figure 2(b)) and the pore volume values reported in Table 2 are lower than those of the 300 and 500 °C biochars, suggesting a reduction in accessible microporous structures at higher thermal treatment.

The assessment of material wettability involved some operational challenges. While the biochar produced at 300 °C could be compacted adequately for contact angle measurements, yielding a value of 118° ± 5 and thus indicating a marked hydrophobic behaviour, the materials pyrolyzed at 500 and 700 °C remained fragile and poorly cohesive even after compression at 13 tonnes. For these samples, the inability to measure a static contact angle is attributed to their highly developed porous structure and limited pellet cohesion, which induces rapid capillary infiltration of water droplets. Elemental analysis confirms progressive structural evolution and changes in intrinsic surface polarity with increasing pyrolysis temperature. The atomic O/C ratio, commonly used as an indicator of surface polarity and oxygen-containing functional groups, decreased from 0.21 at 300 °C to a minimum of 0.12 at 500 °C (Table 2), reflecting substantial deoxygenation under intermediate pyrolysis conditions (Dong *et al.* 2025). The slight increase in O/C at 700 °C (0.16), together with the lowest measured specific surface area, may suggest structural rearrangements and partial collapse or coalescence of accessible micropores at excessive thermal conditions. Nevertheless, as previously reported by Gray *et al.* (2014), capillary forces within biochar pore networks

can enhance water penetration independently of intrinsic surface chemistry, thereby dominating the apparent wettability response and limiting the interpretability of static contact angle measurements in highly porous materials.

3.2. FCM analysis to quantify MPs and bacteria in wastewater

Influent and effluent WW collected from the filtration columns were analyzed using FCM, a single-particle analytical technique detecting multiple optical signals from individual particles as small as 200 nm. Figure 3 shows representative cytograms of WW spiked with 1-μm MPs and stained with SYBR Green I, highlighting the distinct regions corresponding to MPs and bacterial cells. Each dot represents an event detected by the instrument. To optimize discrimination between the two populations, three signals were combined: FSC, SSC, and green fluorescence (BL1). As it is standard in FCM, all axes are reported in arbitrary units (a.u.) and logarithmic scale.

SYBR Green I binds to double-stranded DNA and emits bright green fluorescence, allowing bacterial cells, including both viable and non-viable cells, to be distinguished based on their high BL1 intensity (typically around 10^4–10^5 a.u.). In this study, WW contained approximately 10^8–10^9 cells L^{-1}. In the FSC versus SSC plot (Figure 3(a)), bacterial cells exhibit lower scattering intensities because of their small size and the high-water content that causes the low refractive index. Conversely, 1-μm polystyrene MPs generate stronger scatter signals due to the higher refractive index and the solid and granular structure of these particles. In fluorescence-based cytograms (Figure 3(b) and 3(c)), the BL1 intensity of 1-μm MPs is centred around ~2×10^4 a.u., which overlaps with the wide intensity range of the bacterial cells. Therefore, reliable gating of the two populations requires combining multiple optical parameters, which ensures accurate identification and precise particle enumeration in these complex WW samples.

Despite the small size of the MPs, FCM demonstrated excellent sensitivity and precision in distinguishing them from the surrounding microbial community and inert debris naturally present in WW samples. Currently, no other analytical technique allows such fast, accurate, and high-throughput enumeration of micrometre-scale MPs in complex environmental matrices such as WW (Foladori *et al.* 2025).

3.3. Results obtained in the rapid small-scale column tests

To evaluate the removal performance of the three SCG-biochars, a series of rapid filtration column tests was performed. Prior to MP spiking, each column underwent complete wetting and conditioning to ensure full pore activation and maximize contact between the biochar surface and the suspended microcontaminants. The five-step protocol – including pre-equilibration, WW conditioning, MP spiking, elution, and washing – enabled detailed characterization of both short-term retention and particle release across operational stages. Breakthrough behaviour for the three biochars is summarized in Figure 4, which reports the evolution in the relative concentrations of bacterial cells (Figure 4(a)) and 1-μm MPs (Figure 4(b)) across the operating phases of the filtration tests. Removal efficiencies are summarized in Table 3, together with the percentage of particles washed out from the columns, relative to the amount retained.

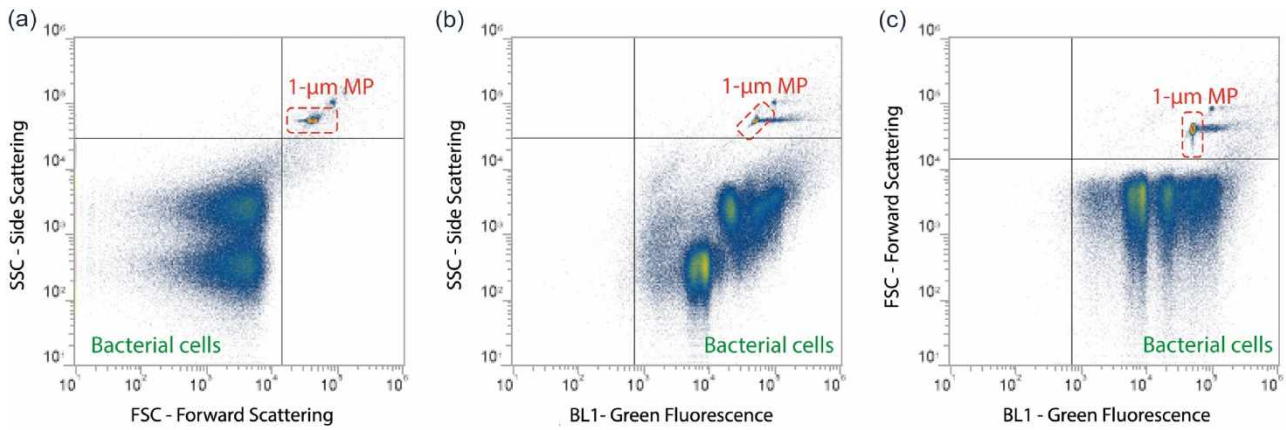

Figure 3 | Representative cytograms of fluorescent 1-μm MPs and SYBR Green I-stained bacterial cells in WW: (a) FSC versus SSC plot distinguishes events on the basis of size, refractive index, and particle structure, (b) BL1 versus SSC, and (c) BL1 versus FSC plots are used to identify events with different fluorescence intensity. All signals on the axes are reported in arbitrary units.

With regards to bacterial cells, the first three PVs represented a transitional phase in which the columns adjusted to influent WW, reaching a stable operational equilibrium after approximately six PVs. Among the materials tested, the 300 °C biochar showed the lowest retention efficiency, capturing only 38 ± 18% of bacteria in influent WW. Removal significantly improved with increasing pyrolysis temperature: the 700 °C biochar retained 56 ± 11% of bacteria ($p < 0.01$), while the 500 °C biochar performed best overall ($p < 0.01$), entrapping 87 ± 9% of cells in influent WW. Washing (phase v) resulted in an immediate release of bacteria from all columns, with effluent concentrations equal to or exceeding the amounts in influent WW (capped at 1 in Figure 4(a)). This release likely reflects microbial colonization of the biochar matrix during filtration, particularly in the 300 °C material, as supported by the marked reduction in carbon content after use (from 67.6 to 31.1%) and by microscopic evidence (Table S1 and Figure S3).

Bacteria and other microorganisms naturally present in the WW matrix can interact with porous adsorbent materials either actively or passively, leading to attachment, retention, and subsequent growth, whose extent depends on the availability of compounds serving as energy or carbon sources, as well as on the surface area available for attachment. In

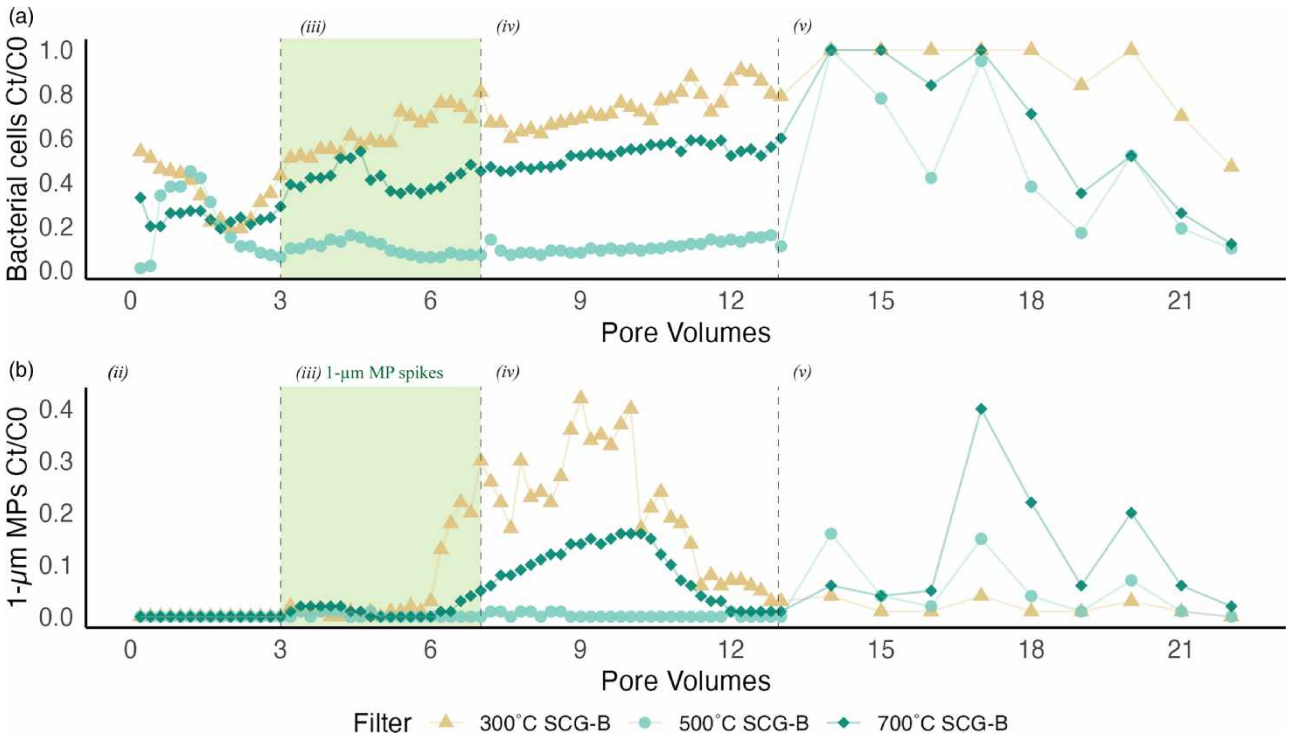

Figure 4 | Breakthrough curves of (a) bacterial cells and (b) 1-μm MPs in three SCG-biochar filtration columns. Filtration tests consisted of five phases, (i) pre-equilibration with 10 PVs of distilled water; (ii) conditioning with three PVs of WW; (iii) spiking with four PVs of WW spiked with 1-μm MPs (0.8 mg L^{-1}); (iv) elution with six PVs of WW; and (v) washing with three PVs of distilled water alternated with air, applied three times.

Table 3 | Removal efficiencies of bacterial cells and 1-μm MPs in three SCG-biochar filtration columns

	Bacterial cells		1-μm MPs	
SCG-biochar	**Removal efficiency (%)**	**Released during washing (%)**	**Removal efficiency (%)**	**Released during washing (%)**
300 °C SCG-B	38 ± 18	−435[a]	73 ± 9	4 ± 1
500 °C SCG-B	87 ± 9	44 ± 29	99.2 ± 0.3	12 ± 6
700 °C SCG-B	56 ± 11	92 ± 29	85 ± 6	32 ± 12

Note: The table reports also the percentage of bacterial cells and MPs released from the biochar columns during washing, relative to the amount retained.
[a]Released amount greater than filtered amount resulting from column colonization.

addition, the hydrophobic character of the surface and the presence of specific functional groups, as in the case of 300 °C biochar, can further enhance microbial adhesion, as commonly observed in granular activated carbon (GAC) filters used for drinking water treatment (Magic-Knezev *et al.* 2009). In particular, materials that are favourable for cellular adhesion, including bacterial attachment, typically exhibit an optimal balance between wettability and moderate hydrophobicity (with contact angles of 40–70° up to about 130°, Yuan *et al.* 2017), whereas extremely hydrophobic or highly hydrophilic surfaces tend to be less readily colonized.

Microbial colonization not only promotes stable attachment but can also alter the physicochemical properties of the adsorbent material: the formation of EPS, rich in polysaccharides and hydrophilic moieties, can generate wetted surface domains (Flemming & Wingender 2010). Consistent with this interpretation, a slight decrease in hydrophobicity was observed for the 300 °C biochar after filtration, with the contact angle decreasing to 114° ± 4, potentially reflecting a contribution from microbial colonization. However, this effect remained modest, resulting in only a minor reduction in the contact angle. In contrast, for the samples produced at 500 and 700 °C, contact angle measurements could not be reliably estimated nor after filtration. Such biofilm-driven surface transformations may help explain the bacterial release observed in biochar columns following washing and underscore the dynamic interplay between microbial activity and adsorbent properties during filtration processes.

Regarding 1-μm MPs (Figure 4(b)), the three columns exhibited significantly different behaviours ($p < 0.01$), although none approached saturation as effluent concentrations consistently remained below the influent ($C_t < C_0$). The 500 °C biochar achieved the highest retention, removing 99.2 ± 0.3% of influent MPs, with very low concentrations of the effluent of the filtration tests. This was followed by the 700 °C material (85 ± 6%), while the 300 °C biochar showed the lowest and most fluctuating removal (73 ± 9%). The instability observed in the 300 °C column is likely due to its limited surface area and less-developed pore structure (Table 2), which remains more similar to that of the raw unheated SCG material (Figure 2). In contrast, the partial collapse of microporosity and the formation of wider pores at 700 °C (presented in Section 3.1) may explain its intermediate performance.

Instead, washing induced only a partial remobilization of MPs from the 500 and 700 °C columns, with release rates of 12 ± 6 and 32 ± 12%, respectively, whereas the 300 °C biochar released only 4 ± 1% of previously retained MPs (Table 3). On the basis of these results, MPs appear more deeply trapped within the biochar pore structure than bacteria, undergoing only a limited resuspension during water and air washing. This behaviour suggests additional physical retention mechanisms beyond simple surface adhesion, as confirmed by SEM evidence (see Section 3.5).

3.4. Results obtained in the long-time filtration column tests

Since the biochar produced at 500 °C exhibited the best simultaneous removal of MPs and bacterial cells during the rapid column tests, it was selected for long-time column experiments to evaluate breakthrough and saturation behaviour. This filtration run was carried out with WW spiked with 1-μm MPs (1.6 mg L^{-1}) and applying up to 50 PVs. The column began releasing detectable MPs only after approximately 10 PVs and reached 50% breakthrough after 50 PVs, corresponding to around 500 min of continuous operation (Figure 5).

Breakthrough data were fitted using both the Yoon–Nelson and Thomas models. Under the classical assumptions of fixed-bed filtration, namely plug flow, Langmuir-type kinetics, constant influent concentration, and negligible axial dispersion (Patel 2019), the two models have identical logistic form and are mathematically equivalent when C_0, Q, and bed mass W are constants, as in this study. The parameters of the two models are related by $k_{YN} = k_{TH}\, C_0$ and $\tau = q_0\, W/(Q\, C_0)$; consequently, the models produced identical fits and overlapping breakthrough curves (Apiratikul & Chu 2021). For operational simplicity, only the Yoon–Nelson model is presented here (Figure 5), with an estimated coefficient of determination $R^2 = 0.92$ and an estimated 50% breakthrough occurring at 464 min (Table 4).

However, in granular fixed-bed columns, the breakthrough curve often exhibits asymmetric or non-ideal behaviour, resulting in a poor fit when modelled using conventional equations such as the Yoon–Nelson and Thomas models (Hu *et al.* 2024). These deviations arise from local mixing and axial dispersion (Knox *et al.* 2016) as well as external film resistance and intraparticle diffusion limitations (Patel 2019). The main limitation of these models lies in their assumption of time-invariant rate constants and transport properties, which fails to capture the pore size distribution of the adsorbent and the evolving diffusive microenvironments that develop as adsorption sites become progressively occupied (Hu *et al.* 2024). Moreover, rapid microbial colonization and bioaggregate formation under pore-scale flow can transiently modify

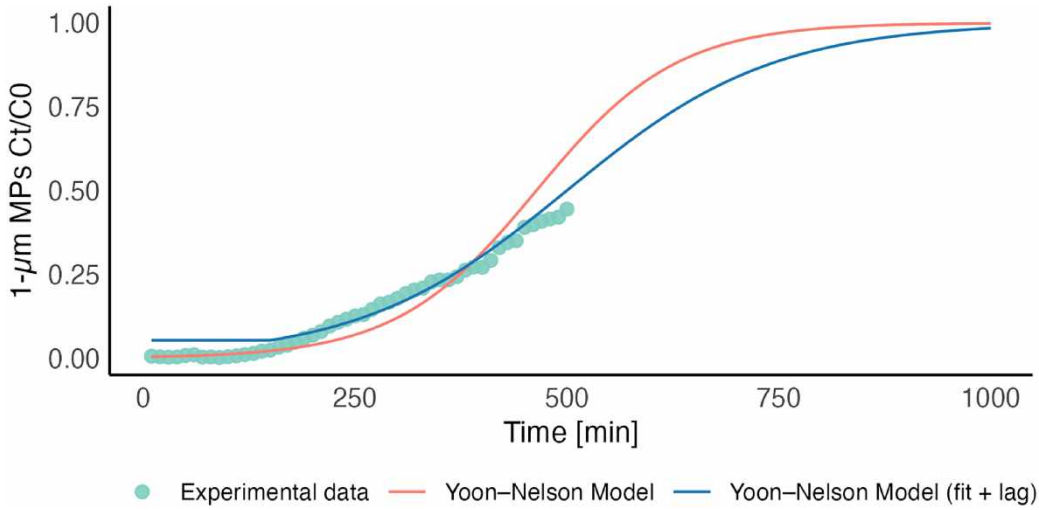

Figure 5 | Experimental breakthrough data of the long-time filtration test (50 PVs of WW spiked with 1-μm MPs at 1.6 mg L^{-1}) fitted with Yoon–Nelson models, with and without lag correction (t_0). The fit + lag model incorporates a hydrodynamic delay estimated with the kinetic parameters to account for void volume and initial non-ideal conditions in the column.

Table 4 | Comparison of kinetic parameters from Yoon–Nelson and Thomas models with and without lag correction (t_0)

	Estimated model parameters					
Model	k_{YN} (min^{-1})	k_{TH} (mL mg^{-1} min^{-1})	t_0 (min)	τ (min)	q_0 (mg g^{-1})	R^2
Yoon–Nelson and Thomas	0.0121	0.0076	–	464	185	0.92
Yoon–Nelson and Thomas fit + lag	0.0082	0.0052	82.6	500	199	0.97

Note: The fit + lag model incorporates a hydrodynamic delay estimated with the kinetic parameters to account for void volume and initial non-ideal conditions in the column.

local hydrodynamics and effective porosity, altering mass transfer dynamics and contributing to early deviations from ideal breakthrough behaviour (Lee *et al.* 2023).

To correct for early-stage non-idealities in model fitting, a lag time (t_0) was introduced and breakthrough data fitted as a function of effective time $t_{eff} = t - t_0$, where t_0 represents a hydrodynamic lag or void volume time, i.e. the time required for the influent to fully penetrate and activate the bed. The parameter t_0 was first estimated by selecting the value that maximized the linearity (R^2) of the log-linear Yoon–Nelson transformation (Apiratikul & Chu 2021) after excluding unstable tails. With t_0 fixed, k_{YN} and τ were subsequently determined by nonlinear least-squares regression, minimizing the residuals between measured and predicted C_t/C_0. This modification effectively translates the logistic breakthrough curve to incorporate the void volume and transient holdup effects, thereby improving both parameter stability and model's coefficient of determination (Table 4). Including the lag term provided a more accurate description of the intrinsic filtration performance, with an improved fit ($R^2 = 0.97$) and a 50% breakthrough now estimated at 500 min, in closer agreement with the experimental data. The corresponding maximum sorption capacity was estimated at approximately 200 mg g^{-1} of biochar.

3.5. Microscopic observation of the retained MPs and bacteria

To elucidate how 1-μm MPs are captured and immobilized within the biochar matrix, samples of biochar were extracted at the end of the filtration tests and examined by SEM (Figure 6). The micrographs revealed the coexistence of multiple retention mechanisms, consistent with those described for larger MPs (Torboli *et al.* 2025) and with the conceptual framework proposed by Wang *et al.* (2020). Specifically, 1-μm MP was observed (Figure 6): (a) trapped deep within the porous structure of the biochar, (b) stuck in the gaps between the filter particles, and (c) entangled by flaky biochar fragments exhibiting colloidal behaviour. These mechanisms correspond to the three morphologically controlled retention pathways described in the literature, as 'trapped', 'stuck', and 'entangled' (Wang *et al.* 2020).

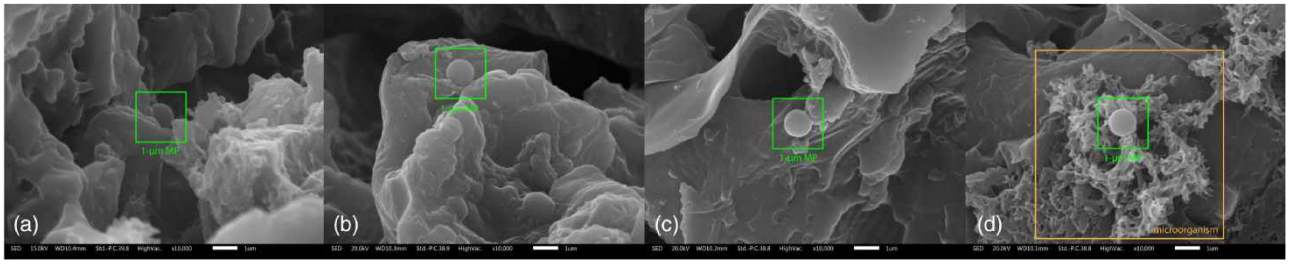

Figure 6 | SEM images of SCG-B with 1-μm MPs: (a) trapped, (b) stuck, (c) entangled, and (d) attached to microorganisms.

In the trapped mechanism, MPs enter larger internal cavities of the biochar but become immobilized within its honeycomb pore channels, typically found in activated carbon and biochar where pore diameters approach the micrometre scale (Abit *et al.* 2014). MPs can also become stuck when they lodge in interparticle gaps or pore openings smaller than their own diameter, effectively making the biochar act as a physical sieve. Consequently, the efficiency of filters in removing MPs is heavily influenced by the granulometry of the filter medium relative to MP size and the pore size distribution. A monomodal porosity may be disadvantageous for filtration applications, as it can lead to excessive size-selective exclusion of the target pollutant. In contrast, a polymodal pore size distribution, particularly evident for the biochar produced at 500 °C, allows multiple entrapment mechanisms to operate simultaneously. This broader pore size variability, together with increased surface area, enhances filtration performance, particularly in complex aqueous matrices containing different pollutants (Jagadeesh & Sundaram 2023). However, whether these structural features also translate into an effective hydrophobic behaviour remains an open question. In highly porous and poorly compacted materials, apparent wetting is dominated by capillary infiltration rather than intrinsic surface chemistry. Therefore, dedicated investigations, such as surface energy analysis or vapour sorption, are required to disentangle the respective roles of porosity and surface chemistry in governing water–material interactions.

Finally, entangled MPs result from interactions with small biochar flakes: although both the MPs and the biochar surfaces are negatively charged, MPs can adhere through short-range van der Waals forces, and they are immobilized either due to an increase in their apparent size or by being wrapped by detached fragments of the filter medium (Wang *et al.* 2020).

Finally, in Figure 6(d), some MPs were found attached to microorganisms also captured within the column, indicating that microbial colonisation can further contribute to their immobilisation. SEM evidence confirms that these mechanisms act simultaneously, even at the micrometre scale, enhancing MP retention beyond simple surface interaction and explaining the limited desorption observed during washing.

3.6. Study limitations and practical implications

The column configuration implemented in this study closely resembles conventional filtration systems used in WWTPs as tertiary and quaternary stages, typically based on sand, GAC, or synthetic resins. The use of low-cost biochar as a filling material offers a sustainable alternative capable of reducing both MPs and bacteria in secondary-treated WW, supporting reclamation uses. Recent literature confirms the growing interest in biochar for MP removal; however, most available studies focus on relatively large particles or batch adsorption systems (Li *et al.* 2024; Chandravanshi *et al.* 2026), while investigations specifically addressing 1-μm MPs under dynamic flow conditions remain limited. A key bottleneck in this field is the lack of standardized methods for detecting and quantifying micrometric MPs in real WW, where concentrations are often low, highly variable, and poorly characterized. This variability hinders accurate estimation of maximum removal rates and complicates the study of their kinetics and transport in full-scale systems. Moreover, environmental MPs are typically subjected to ageing, oxidation, and biofilm formation, which may alter surface hydrophilicity and modify electrostatic interactions. These transformations may influence retention behaviour compared with the fluorescent polystyrene microspheres used here as surrogate particles. The lack of results for very small MPs makes it difficult, at present, to compare our findings with those of other conventional systems. Nevertheless, the lesson learned from this research, using spiked 1-μm-MPs, underscores the importance of evaluating the removal efficiency of particles a few micrometres in size, as their removal appears more difficult (Parashar & Hait 2024; Torboli *et al.* 2025). In fact, the focus on the 1-μm size fraction addresses a particularly challenging transport regime in which attachment efficiency declines and purely mechanical

straining becomes less effective. In view of further development, the small-scale dynamic column conditions used in our study with temperature-optimized biochar and real secondary-treated WW resulted in a representative configuration due to enhanced mass transfer and continuous operation (as indicated also by Chandravanshi *et al.* (2026)). This suggests the possibility to generalize the results. The proposed system, due to the similarity with conventional filtration columns, suggests the potential for retrofitting existing infrastructure rather than requiring complete redesign. However, given future scale-up, the scalability of biochar production from waste biomass may be limited at present and warrants further research.

4. CONCLUSIONS

This study demonstrates how tuning pyrolysis temperature can optimize biochar properties for the removal of small MPs in real WW matrices. By integrating controlled MP spiking with high-throughput FCM and rapid small-scale column testing, we provide a reproducible framework to evaluate removal performance at the challenging 1-μm scale, addressing a current methodological gap in MP treatment research.

Among the tested materials, biochar produced at 500 °C exhibited the highest removal efficiency, achieving nearly complete retention of 1-μm MPs while maintaining substantial bacterial removal. This temperature emerged as a condition at which structural development and removal performance were maximized, due to enhanced surface area, balanced surface polarity, and a polymodal pore size distribution supporting multiple retention mechanisms. In contrast, further thermal intensification reduced the availability of accessible pore structures relevant for particle retention. Although intermediate temperatures (e.g., 400 or 600 °C) could further refine the optimal operating point, these findings contribute to the growing body of literature on biochar-based filtration by demonstrating that an energy-efficient pyrolysis range can be identified to maximize removal performance while converting waste biomass into a high-value filtration medium.

Moreover, further improvements are possible. The study employed fluorescent polystyrene microspheres as surrogate particles, which, although representative of small MPs that typically evade conventional treatments, do not capture the full diversity of environmental MPs. Future research should evaluate naturally occurring MPs of heterogeneous composition, morphology, and ageing state, and investigate the long-term stability of filtration media. In particular, further studies are needed to clarify how surface transformations of environmental MPs influence retention behaviour and to better disentangle the respective contributions of porosity and surface chemistry in governing particle–material interactions. By integrating a controlled 1-μm MP tracer framework with dynamic column testing, the combined analytical–engineering approach proposed here can support the rational design and optimization of scalable, low-cost biochar filtration units for tertiary or quaternary WW treatment applications.

ACKNOWLEDGEMENTS

We thank Lorena Maines of the Microstructural Analysis Laboratory, Department of Industrial Engineering, University of Trento, for performing the SEM imaging. We also thank Wilma Vaona of the Laboratory of Materials for Engineering and Energy, Department of Civil, Environmental and Mechanical Engineering, University of Trento, for performing the elemental composition analyses. Finally, we sincerely thank Lukasz Niedzwiecki of the Green Processes Engineering – Biomass Lab, Department of Civil, Environmental and Mechanical Engineering, University of Trento, for performing the ash content analyses.

AUTHORS CONTRIBUTIONS

AT: conceptualization, methodology, formal analysis, and writing original draft; LF: conceptualization, methodology, and writing – review and editing; RC: methodology, writing – review and editing; DM: formal analysis, methodology; LB: methodology; PF: conceptualization, methodology, writing – review and editing, project administration.

DECLARATION OF GENERATIVE AI AND AI-ASSISTED TECHNOLOGIES IN THE WRITING PROCESS

During the preparation of this work, the authors used ChatGPT to enhance the readability and language of this manuscript. After using this tool, the authors carefully reviewed and edited the content as needed, assuming full responsibility for the content of the publication.

DATA AVAILABILITY STATEMENT

All relevant data are included in the paper or its Supplementary Information.

CONFLICT OF INTEREST

The authors declare there is no conflict.

REFERENCES

Abit, S. M., Bolster, C. H., Cantrell, K. B., Flores, J. Q. & Walker, S. L. (2014) Transport of *Escherichia coli*, *Salmonella typhimurium*, and microspheres in biochar-amended soils with different textures, *Journal of Environmental Quality*, **43**, 371–388. https://doi.org/10.2134/jeq2013.06.0236.

Adhikari, S., Kelkar, V., Kumar, R. & Halden, R. U. (2022) Methods and challenges in the detection of microplastics and nanoplastics: a mini-review, *Polymer International*, **71** (5), 543–551. https://doi.org/10.1002/pi.6348.

Ali, S. S., Elsamahy, T., Al-Tohamy, R. & Sun, J. (2024) A critical review of microplastics in aquatic ecosystems: degradation mechanisms and removing strategies, *Environmental Science and Ecotechnology*, **21**, 100427. https://doi.org/10.1016/j.ese.2024.100427.

Apiratikul, R. & Chu, K. H. (2021) Improved fixed bed models for correlating asymmetric adsorption breakthrough curves, *Journal of Water Process Engineering*, **40**, 101810. https://doi.org/10.1016/j.jwpe.2020.101810.

Bhagwat, G., O'Connor, W., Grainge, I. & Palanisami, T. (2021) Understanding the fundamental basis for biofilm formation on plastic surfaces: role of conditioning films, *Frontiers in Microbiology*, **12**, 687118. https://doi.org/10.3389/fmicb.2021.687118.

Cairns, S., Meza-Rojas, D., Holliman, P. J. & Robertson, I. (2024) Interactions between biochar and nano(micro)plastics in the remediation of aqueous media, *International Journal of Environmental Research*, **18**, 87. https://doi.org/10.1007/s41742-024-00635-0.

Chandravanshi, R., Tiwari, A., Tiwari, A., Dubey, R. & Pandey, S. K. (2026) Biochar as an adsorbent for microplastics present in aquatic environments: a comparative review between batch and column adsorption, *Journal of Environmental Chemical Engineering*, **14** (3), 122530. https://doi.org/10.1016/j.jece.2026.122530.

Cook, S., Chan, H.-L., Abolfathi, S., Bending, G. D., Schäfer, H. & Pearson, J. M. (2020) Longitudinal dispersion of microplastics in aquatic flows using fluorometric techniques, *Water Research*, **170**, 115337. https://doi.org/10.1016/j.watres.2019.115337.

Costigan, E., Collins, A., Hatinoglu, M. D., Bhagat, K., MacRae, J., Perreault, F. & Apul, O. (2022) Adsorption of organic pollutants by microplastics: overview of a dissonant literature, *Journal of Hazardous Materials Advances*, **6**, 100091. https://doi.org/10.1016/j.hazadv.2022.100091.

Dong, H., Yi, H., Chen, S., Guo, J., Zhao, F., Belver, C., Yuan, H., Liang, B., Gao, G., Guan, J., Nesic, A. & Bedia, J. (2025) Reed biochar by microwave-assisted pyrolysis for the removal of tetracycline in water, *Environmental Research*, **285**, 122518. https://doi.org/10.1016/j.envres.2025.122518.

Dronjak, L., Exposito, N., Sierra, J., Schuhmacher, M., Florencio, K., Corzo, B. & Rovira, J. (2023) Tracing the fate of microplastic in wastewater treatment plant: a multi-stage analysis of treatment units and sludge, *Environmental Pollution*, **333**, 122072. https://doi.org/10.1016/j.envpol.2023.122072.

Dykes, C., Pearson, J., Bending, G. & Abolfathi, S. (2026) Biofilm growth is insufficient to retain large buoyant microplastics in constructed wetlands, *Journal of Hazardous Materials*, **504**, 141265. https://doi.org/10.1016/j.jhazmat.2026.141265.

Fady, P.-E., Richardson, A. K., Barron, L. P., Mason, A. J., Volpe, R. & Barr, M. R. (2025) Biochar filtration of drug-resistant bacteria and active pharmaceutical ingredients to combat antimicrobial resistance, *Scientific Reports*, **15**, 1256. https://doi.org/10.1038/s41598-024-83825-2.

Flemming, H.-C. & Wingender, J. (2010) The biofilm matrix, *Nature Reviews Microbiology*, **8**, 623–633. https://doi.org/10.1038/nrmicro2415.

Flemming, H.-C., Van Hullebusch, E. D., Neu, T. R., Nielsen, P. H., Seviour, T., Stoodley, P., Wingender, J. & Wuertz, S. (2023) The biofilm matrix: multitasking in a shared space, *Nature Reviews Microbiology*, **21**, 70–86. https://doi.org/10.1038/s41579-022-00791-0.

Foladori, P., Torboli, A. & Bruni, L. (2025) Can flow cytometry emerge as a high-throughput technique for micro- and nanoplastics analysis in complex environmental aqueous matrices? *Bioresource Technology Reports*, **31**, 102170. https://doi.org/10.1016/j.biteb.2025.102170.

Gray, M., Johnson, M. G., Dragila, M. I. & Kleber, M. (2014) Water uptake in biochars: the roles of porosity and hydrophobicity, *Biomass and Bioenergy*, **61**, 196–205. https://doi.org/10.1016/j.biombioe.2013.12.010.

Guo, M., Noori, R. & Abolfathi, S. (2024) Microplastics in freshwater systems: dynamic behaviour and transport processes, *Resources, Conservation and Recycling*, **205**, 107578. https://doi.org/10.1016/j.resconrec.2024.107578.

Hajji, S., Ben-Haddad, M., Abelouah, M. R., De-la-Torre, G. E. & Alla, A. A. (2023) Occurrence, characteristics, and removal of microplastics in wastewater treatment plants located on the Moroccan Atlantic: the case of Agadir metropolis, *Science of the Total Environment*, **862**, 160815. https://doi.org/10.1016/j.scitotenv.2022.160815.

Harvey, O. R., Herbert, B. E., Kuo, L.-J. & Louchouarn, P. (2012) Generalized two-dimensional perturbation correlation infrared spectroscopy reveals mechanisms for the development of surface charge and recalcitrance in plant-derived biochars, *Environmental Science & Technology*, **46** (19), 10641-10650. https://doi.org/10.1021/es302971d.

Hidayaturrahman, H. & Lee, T.-G. (2019) A study on characteristics of microplastic in wastewater of South Korea: identification, quantification, and fate of microplastics during treatment process, *Marine Pollution Bulletin*, **146**, 696–702. https://doi.org/10.1016/j.marpolbul.2019.06.071.

Hsieh, L., He, L., Zhang, M., Lv, W., Yang, K. & Tong, M. (2022) Addition of biochar as thin preamble layer into sand filtration columns could improve the microplastics removal from water, *Water Research*, **221**, 118783. https://doi.org/10.1016/j.watres.2022.118783.

Hu, Q., Yang, X., Huang, L., Li, Y., Hao, L., Pei, Q. & Pei, X. (2024) A critical review of breakthrough models with analytical solutions in a fixed-bed column, *Journal of Water Process Engineering*, **59**, 105065. https://doi.org/10.1016/j.jwpe.2024.105065.

Iordachescu, L., Papacharalampos, K., Barritaud, L., Denieul, M.-P., Plessis, E., Baratto, G., Julien, V. & Vollertsen, J. (2024) Microplastics in an advanced wastewater treatment plant: sustained and robust removal rates unfazed by seasonal variations, *Microplastics and Nanoplastics*, **4**, 18. https://doi.org/10.1186/s43591-024-00097-3.

Ippolito, J. A., Cui, L., Kammann, C., Wrage-Mönnig, N., Estavillo, J. M., Fuertes-Mendizabal, T., Cayuela, M. L., Sigua, G., Novak, J., Spokas, K. & Borchard, N. (2020) Feedstock choice, pyrolysis temperature and type influence biochar characteristics: a comprehensive meta-data analysis review, *Biochar*, **2**, 421–438. https://doi.org/10.1007/s42773-020-00067-x.

Jagadeesh, N. & Sundaram, B. (2023) Adsorption of pollutants from wastewater by biochar: a review, *Journal of Hazardous Materials Advances*, **9**, 100226. https://doi.org/10.1016/j.hazadv.2022.100226.

Ji, G., Xing, Y. & You, T. (2024) Biochar as adsorbents for environmental microplastics and nanoplastics removal, *Journal of Environmental Chemical Engineering*, **12**, 113377. https://doi.org/10.1016/j.jece.2024.113377.

Jia, J., Liu, Q., Zhao, E., Li, X., Xiong, X. & Wu, C. (2024) Biofilm formation on microplastics and interactions with antibiotics, antibiotic resistance genes and pathogens in aquatic environment, *Eco-Environment & Health*, **3**, 516–528. https://doi.org/10.1016/j.eehl.2024.05.003.

Knox, J. C., Ebner, A. D., LeVan, M. D., Coker, R. F. & Ritter, J. A. (2016) Limitations of breakthrough curve analysis in fixed-bed adsorption, *Industrial & Engineering Chemistry Research*, **55**, 4734–4748. https://doi.org/10.1021/acs.iecr.6b00516.

Kuloglija, S., Kropik, I.-M., Ahmed, A. E. G., Kalman, V., Windbacher, A., Jordan, C., Konior, A., Abbaspour, N., Steinacher, N., Winter, F., Tomasetig, D., Lamprinidou, E. & Harasek, M. (2026) Isotherms and kinetics of CO_2 adsorption on biochar-based activated carbon for sustainable climate solutions, *Separation and Purification Technology*, **382**, 136079. https://doi.org/10.1016/j.seppur.2025.136079.

Lee, S. H., Secchi, E. & Kang, P. K. (2023) Rapid formation of bioaggregates and morphology transition to biofilm streamers induced by pore-throat flows, *Proceedings of the National Academy of Sciences*, **120**, e2204466120. https://doi.org/10.1073/pnas.2204466120.

Li, W., Xing, Y., Guo, Y., Zhang, D., Tang, Y., Chen, J., Zhang, H. & Jiang, B. (2024) The removal and mitigation effects of biochar on microplastics in water and soils: application and mechanism analysis, *Sustainability*, **16**, 9749. https://doi.org/10.3390/su16229749.

Liu, W., Zhang, J., Liu, H., Guo, X., Zhang, X., Yao, X., Cao, Z. & Zhang, T. (2021) A review of the removal of microplastics in global wastewater treatment plants: characteristics and mechanisms, *Environment International*, **146**, 106277. https://doi.org/10.1016/j.envint.2020.106277.

Magic-Knezev, A., Wullings, B. & Van Der Kooij, D. (2009) *Polaromonas* and *Hydrogenophaga* species are the predominant bacteria cultured from granular activated carbon filters in water treatment, *Journal of Applied Microbiology*, **107**, 1457–1467. https://doi.org/10.1111/j.1365-2672.2009.04337.x.

Monira, S., Roychand, R., Hai, F. I., Bhuiyan, M., Dhar, B. R. & Pramanik, B. K. (2023) Nano and microplastics occurrence in wastewater treatment plants: a comprehensive understanding of microplastics fragmentation and their removal, *Chemosphere*, **334**, 139011. https://doi.org/10.1016/j.chemosphere.2023.139011.

Olubusoye, B. S., Cizdziel, J. V., Wontor, K., Heinen, E., Grandberry, T., Bennett, E. R. & Moore, M. T. (2024) Removal of microplastics from agricultural runoff using biochar: a column feasibility study, *Frontiers in Environmental Science*, **12**, 1388606. https://doi.org/10.3389/fenvs.2024.1388606.

Ormaniec, P. (2024) Occurrence and analysis of microplastics in municipal wastewater, Poland, *Environmental Science and Pollution Research*, **31**, 49646–49655. https://doi.org/10.1007/s11356-024-34488-z.

Parashar, N. & Hait, S. (2024) Cetyl trimethyl ammonium bromide-modified magnetic biochar-integrated sand filter for microplastics removal from secondary-treated sewage effluents: performance evaluation and mechanistic insights, *Journal of Water Process Engineering*, **59**, 105035. https://doi.org/10.1016/j.jwpe.2024.105035.

Patel, H. (2019) Fixed-bed column adsorption study: a comprehensive review, *Applied Water Science*, **9**, 45. https://doi.org/10.1007/s13201-019-0927-7.

Reza, T., Mohamad Riza, Z. H., Sheikh Abdullah, S. R., Abu Hasan, H., Ismail, N. & Othman, A. R. (2023) Microplastic removal in wastewater treatment plants (WWTPs) by natural coagulation: a literature review, *Toxics*, **12**, 12. https://doi.org/10.3390/toxics12010012.

Rummel, C. D., Jahnke, A., Gorokhova, E., Kühnel, D. & Schmitt-Jansen, M. (2017) Impacts of biofilm formation on the fate and potential effects of microplastic in the aquatic environment, *Environmental Science & Technology Letters*, **4**, 258–267. https://doi.org/10.1021/acs.estlett.7b00164.

Stalder, A. F., Kulik, G., Sage, D., Barbieri, L. & Hoffmann, P. (2006) A snake-based approach to accurate determination of both contact points and contact angles, *Colloids and Surfaces A: Physicochemical and Engineering Aspects*, **286**, 92–103. https://doi.org/10.1016/j.colsurfa.2006.03.008.

Thomas, H. C. (1944) Heterogeneous ion exchange in a flowing system, *Journal of the American Chemical Society*, **66**, 1664–1666. https://doi.org/10.1021/ja01238a017.

Thommes, M., Kaneko, K., Neimark, A. V., Olivier, J. P., Rodriguez-Reinoso, F., Rouquerol, J. & Sing, K. S. W. (2015) Physisorption of gases, with special reference to the evaluation of surface area and pore size distribution (IUPAC technical report), *Pure and Applied Chemistry*, **87**, 1051–1069. https://doi.org/10.1515/pac-2014-1117.

Tomczyk, A., Sokołowska, Z. & Boguta, P. (2020) Biochar physicochemical properties: pyrolysis temperature and feedstock kind effects, *Reviews in Environmental Science and Bio/Technology*, **19**, 191–215. https://doi.org/10.1007/s11157-020-09523-3.

Torboli, A., Foladori, P. & Bruni, L. (2025) Enhanced removal of small microplastics (1–5 μm) from secondary-treated wastewater using spent coffee grounds biochar: application of flow cytometry, *Journal of Water Process Engineering*, **71**, 107270. https://doi.org/10.1016/j.jwpe.2025.107270.

Wang, J. & Wang, S. (2019) Preparation, modification and environmental application of biochar: a review, *Journal of Cleaner Production*, **227**, 1002–1022. https://doi.org/10.1016/j.jclepro.2019.04.282.

Wang, Z., Sedighi, M. & Lea-Langton, A. (2020) Filtration of microplastic spheres by biochar: removal efficiency and immobilisation mechanisms, *Water Research*, **184**, 116165. https://doi.org/10.1016/j.watres.2020.116165.

Wang, L., Li, X., Huang, J., Tuo, J., Li, X., Qian, X. & Abolfathi, S. (2024) The operating performance of modified basalt fibers (MBF) bio-nest reactor exposed to nano-plastics, *Journal of Hazardous Materials*, **480**, 136042. https://doi.org/10.1016/j.jhazmat.2024.136042.

Windsor, F. M., Durance, I., Horton, A. A., Thompson, R. C., Tyler, C. R. & Ormerod, S. J. (2019) A catchment-scale perspective of plastic pollution, *Global Change Biology*, **25** (4), 1207–1221. https://doi.org/10.1111/gcb.14572.

Yoon, Y. H. & Nelson, J. H. (1984) Application of gas adsorption kinetics I. A theoretical model for respirator cartridge service life, *American Industrial Hygiene Association Journal*, **45** (8), 509–516. https://doi.org/10.1080/15298668491400197.

Yuan, Y., Hays, M. P., Hardwidge, P. R. & Kim, J. (2017) Surface characteristics influencing bacterial adhesion to polymeric substrates, *RSC Advances*, **7**, 14254–14261. https://doi.org/10.1039/C7RA01571B.

Zettler, E. R., Mincer, T. J. & Amaral-Zettler, L. A. (2013) Life in the 'plastisphere': microbial communities on plastic marine debris, *Environmental Science & Technology*, **47**, 7137–7146. https://doi.org/10.1021/es401288x.

Zhang, Y., Jiang, H., Bian, K., Wang, H. & Wang, C. (2021) A critical review of control and removal strategies for microplastics from aquatic environments, *Journal of Environmental Chemical Engineering*, **9**, 105463. https://doi.org/10.1016/j.jece.2021.105463.

Ziajahromi, S., Neale, P. A., Rintoul, L. & Leusch, F. D. L. (2017) Wastewater treatment plants as a pathway for microplastics: development of a new approach to sample wastewater-based microplastics, *Water Research*, **112**, 93–99. https://doi.org/10.1016/j.watres.2017.01.042.

First received 26 February 2026; accepted in revised form 25 May 2026. Available online 12 June 2026